RESEARCH PAPER

CrossMark

Study on the statistical intensity distribution (SID) of fluorescent nanoparticles in TIRFM measurement

Xu Zheng[1] · Fei Shi[1] · Zhanhua Silber-Li[1]

Abstract

Total internal reflection fluorescence microscopy (TIRFM) based on the evanescent wave provides a powerful imaging tool to measure nanoparticle dynamics near the interfaces in nanofluidic and biophysical systems. The most dramatic advantage of this technique is encoding the nanoparticle motion in the vertical dimension into intensity variation. However, large measurement uncertainty was found in previous works, which has been a major obstacle for applying TIRFM to nanofluidic studies. In this study, we investigate the statistical intensity distribution (SID) of the fluorescent nanoparticles in the evanescent field. We establish a theoretical description of the SID by considering the Boltzmann distribution of the nanoparticle concentration, the statistical particle size variation, and the focal plane thickness of the objective. The theoretical results show excellent agreement with the experimental SID histogram. We then develop a method to precisely determine the base intensity I_0 and decode the vertical positions of nanoparticles, by which the measurement uncertainty of TIRFM can be significantly reduced. This SID method is verified by the nanoparticle tracking velocimetry measurement near the wall using nanoparticles with diameters of 100 nm or 250 nm as tracers. Furthermore, our experiments show that the SID of nanoparticles is sensitive to the salt concentration of the solution and the nanoparticle properties, implying the possibility of using SID as a nano-probe to explore solution or colloidal properties in nanofluidics.

Keywords TIRFM · Nanoparticles · Statistical intensity distribution (SID) · NanoPIV/PTV

1 Introduction

An evanescent wave is created at the interface between two materials with different refraction indices (for example, glass–water) via total internal reflection of an excitation laser beam. Total internal reflection fluorescent microscopy (TIRFM) utilizes this evanescent wave to illuminate a field with several-hundred-nanometre thickness in the

✉ Xu Zheng
zhengxu@lnm.imech.ac.cn

[1] State Key Laboratory of Nonlinear Mechanics,
Institute of Mechanics, Chinese Academy of Sciences,
Beijing 100190, China

low refractive index fluid. Therefore, when compared with the common volume-illuminating microscopy, TIRFM can achieve a much better signal–noise ratio and an excellent resolution (Zetterner and Yoda 2003; Huang et al. 2006; Wereley and Meinhart 2010; Chan and Ohl 2012; Li et al. 2014). The evanescent field intensity $I(z)$ of the TIRFM decays exponentially with the distance z from the interface (Prieve and Frej 1990):

$$I(z) = I_0 \exp(-z/d_p), \tag{1}$$

where I_0 is the base intensity at the interface, $d_p = \lambda / \left(4\pi\sqrt{n_1^2\sin^2\theta - n_2^2}\right)$ is the evanescent wave penetration depth, λ is the wavelength of the incident light, θ is the light incident angle, and n_1 and n_2 are the refraction indices of the glass and water, respectively. Obviously, the intensity $I(z)$ in the evanescent field is dependent on its elevation z from the interface. When a nanoparticle locates in the evanescent field, its scattered intensity should also follow the same exponential decay based on Eq. (1). Thus, it is possible to 'decode' the vertical position z of the particle from its

intensity in TIRFM measurements, which is a significant advantage compared with common optical microscopy. However, the parameter I_0 in Eq. (1) referring to the intensity of incident light at the interface is unknown in the measurement, which has caused major difficulty for decoding nanoparticle z positions in TIRFM applications (McKee et al. 2005; Hertlein et al. 2008; Wang et al. 2011; Li et al. 2014; Wang and Huang 2016).

Recently, the TIRFM technique has been introduced into many microfluidic and nanofluidic experiments (Wereley and Meinhart 2010; Squires 2017; Shin et al. 2016). For instance, the investigation of the hindered Brownian motion of nanoparticles near a wall (Kihm et al. 2004; Banerjee and Kihm 2005; Choi et al. 2007; Fan et al. 2015), the slip velocity at the interface (Huang et al. 2006; Bouzigues et al. 2008; Yoda and Kazoe 2011; Qian et al. 2015), and the DLVO (DLVO theory is named after Boris Derjaguin, Lev Landau, Evert Verwey and Theodor Overbeek and describes the force between charged surfaces interacting through a liquid medium. The DLVO force combines the effects of the van der Waals attraction and the electrostatic repulsion in the electric double layer.) force measurement (Wu and Bevan 2005; Madariaga-Marcos et al. 2018) became possible by relying on decoding the z information from the intensity. Wide application prospects of using the TIRFM technique have also been exhibited in biophysics studies and other interdisciplinary fields (Zheng et al. 2018; Bliokh et al. 2014). All of these measurements require a high precision in determining nanoparticle z positions. Thus, overcoming the uncertainty of the base intensity at the interface I_0 becomes a crucial challenge that urgently needs to be solved (Li et al. 2014; Wang and Huang 2016).

To overcome this problem, researchers turned their attention to determining a reference intensity at the interface to represent the base intensity I_0 in Eq. (1). One commonly used approach was using the average intensity of bright nanoparticles attached to a wall to represent I_0. However, this treatment could introduce significant errors in calculating z positions (Bouzigues et al. 2008; Kazoe and Yoda 2011). Moreover, as the nanoparticle intensity is proportional to the amount of fluorophores in the particle volume, i.e., $I \sim d^3$ (where d is the diameter of the particle), the nanoparticle size variation becomes an important factor. Yoda and Kazoe (2011) pointed out that, although the size variation was as small as 6% (for 100-nm particles) in their NanoPIV (Nano Particle Image Velocimetry, a PIV technique with illumination based on the evanescent wave) measurements, the uncertainty of determining z positions could be more than 20%. Thus, effective determination of the base intensity I_0 is one of the most crucial preconditions to obtain the precise nanoparticle z position in TIRFM experiments. Lately, new attempts have been made to understand the physical factors that influence the observed intensity of nanoparticles.

Rich physics has been unveiled in the evanescent field considering the Boltzmann distribution of the nanoparticle concentration, the properties of nanoparticles and the interaction between particles and the wall (Wang et al. 2011; Wang and Huang 2016). These results shed light on a better understanding of the nanoparticle–interface interaction and the development of new methods to solve the problem of determining I_0 and decoding the corresponding z position, although the analysis and calculation are still complex and difficult.

Therefore, in view of the fact that only the intensities of the fluorescent nanoparticles are the "raw data" in TIRFM measurements, this paper focuses on describing the statistical intensity distribution (SID) of all the nanoparticles emerging in the evanescent field near the interface. We develop a method based on the SID to determine I_0 and thus decode the vertical z position of every observed nanoparticle. Being verified by nanoPTV (nano-particle tracking velocimetry) measurements, this SID method significantly reduces the uncertainty compared to previous methods. As a future application of the present method, we will further demonstrate the possibility of using SID as a nano-probe to detect surface properties in nanofluidics.

2 Experimental setup and method

2.1 TIRFM system

The experiment was performed with an objective-based TIRFM system established in an Olympus IX71 microscope with a 100×/NA = 1.45 objective (where NA is the numerical aperture of the objective), as shown in Fig. 1a. A 488-nm laser (Compass, rated power of 150 mW) was introduced by an optical fibre (the power at the fibre exit was approximately 70 mW in the experiment). The incident angle of the laser was adjusted to the critical incident angle θ_{cr} by a micrometer. We calibrated the critical incident angle with a setup utilizing a semi-cylindrical glass prism (section S1 of the Online Resource ESM_1.pdf). The measured θ_{cr} was approximately $61.5° \pm 0.1°$, and the corresponding penetration depth of the evanescent field was approximately $d_p \approx 280$ nm.

2.2 Nanoparticles and solutions

Considering the difficulty of maintaining stable conductivity or Debye length in pure water (18.2 MΩ·cm), the experiments were performed in NaCl solutions with different concentrations (nominally 0.1 mM, 1 mM and 5 mM). The conductivities of these three NaCl solutions were measured to be 10.9 μs/cm, 104.3 μs/cm and 505.1 μs/cm, respectively, by a conductivity meter (Mettler Toledo S40). Thus,
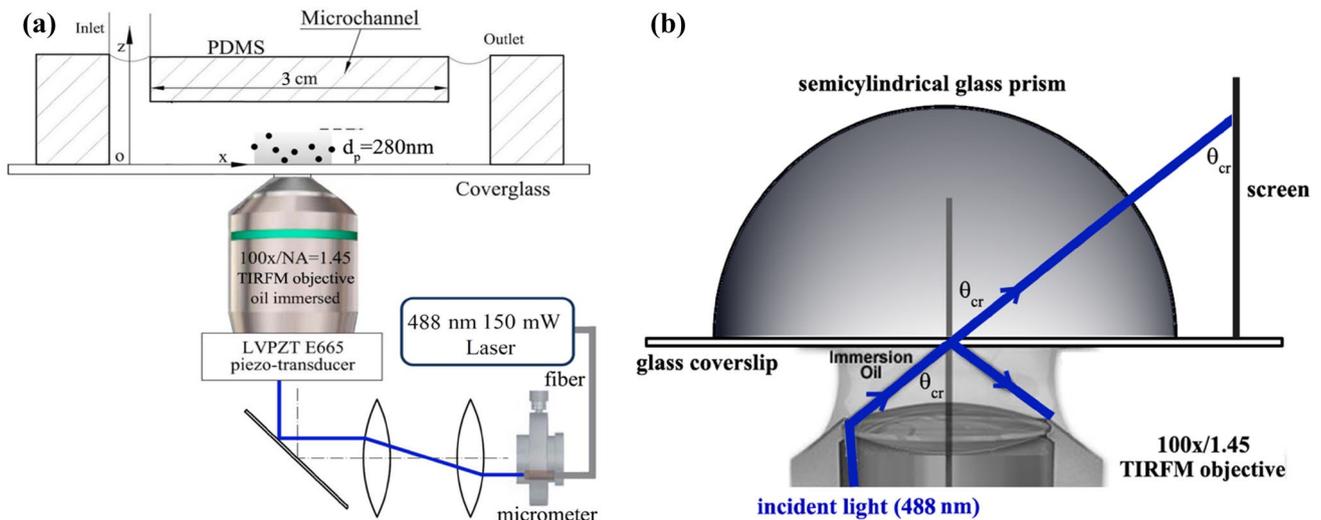
Fig. 1 Schematic diagrams of **a** the TIRFM experimental system and **b** the calibration of the critical incident angel based on a semi-cylindrical prism

the corresponding salt concentrations were approximately 0.094 mM, 0.93 mM and 4.5 mM, respectively; the Debye lengths were 31.4 nm, 10.0 nm and 4.6 nm, respectively. The fluorescent polystyrene (PS) nanoparticles were added to the above NaCl solutions to a particle volumetric concentration of approximately 0.002%. These fluorescent nanoparticles were produced by Thermo Fisher Scientific (diameter 100 nm or 250 nm). We measured the particle size d, the size standard deviation (d_σ) and the particle surface potential ψ_p using a Malvern Zetasizer (Table 1). The size variations σ of the 250-nm and 100-nm particles were calculated to be approximately 1.0% and 6.5%, respectively. During the experiment, the environmental temperature was approximately 19–21 °C, and the relative humidity was approximately 20–40%.

2.3 Experimental observations

A sensitive EMCCD (electron-multiplying charge-coupled device, Andor 897, 512 × 512 pixels) was used to record images. Working with a 100 × objective, the size of a single pixel in the image was approximately 160 nm.

The experiment was performed in a sub-image mode in which the image field of view was fixed at 150 × 80 pixels (approximately 24.0 × 10.8 μm). The observation was performed in a PDMS (polydimethylsiloxane) microchannel (cross section: width $w = 56.0$ μm, height $h = 19.2$ μm, and channel length $L = 3.0$ cm, Zheng and Silber-Li 2008). The measured region was located close to the glass surface in the channel centre. Before the measurement, the prepared experimental solution was injected into the microchannel and, with the help of a piezo-transducer (Physik Instrumente) mounted under the objective, the focal plane was moved to the glass surface (Bouzigues et al. 2008; Zheng and Silber-Li 2008; Joseph and Tabeling 2005). After the experiment started, the EMCCD recorded the image series with an interval time between two frames of $\Delta t_{int} = 7$ ms and an exposure time of $t_e = 0.4$ ms. The observations were performed on 15–25 positions near the interface. At each position, an image series containing 1000 frames was captured. To avoid photobleaching by excessive laser illumination, the total time of capturing 1000 frames lasted only 7 s at each position (section S2 of the Online Resource ESM_1.pdf).

Table 1 Measured parameters of the nanoparticles

	Salt concentration (mM)	Diameter d (nm)	Size std d_σ (nm)	Particle surface potential ψ_p (mV)
φ100 nm	0.094	105.1	± 7.4	− 49.2
	0.93	103.5	± 6.5	− 46.5
	4.5	103.0	± 6.1	− 44.8
φ250 nm	0.094	262.0	± 2.8	− 55.2
	0.93	260.3	± 2.6	− 48.7
	4.5	258.7	± 2.6	− 41.3

2.4 Image processing

We developed a homemade Matlab program for image processing. The image processing contained three procedures: (1) image filtering; (2) particle identification; and (3) determining the centre position and greyscale value of each nanoparticle. Figure 2a shows three successive images of two 100-nm particles. Since there was no background flow, these two nanoparticles only experienced random Brownian motion. The intensity variation in the images represented the change in the vertical z position of each individual particle (Online Resource ESM_2.avi and ESM_3.avi). The image filtering was used to reduce the image noise. Because of the excellent signal-to-noise ratio of the TIRFM images (Fig. 2a), using a proper threshold greyscale value higher than the background intensity was sufficient to remove the background noise. After that, during particle identification the program would first calculate the intensity distribution and the contour map of each nanoparticle (Fig. 2b). The image background greyscale value, which was approximately 300 according to Fig. 2b, was then subtracted from every image in the following processing. A central region (3×3 pixels) in the contour map was considered to be the nanoparticle, and the maximum greyscale value in each region was recorded as the intensity of the corresponding nanoparticle. After identifying the nanoparticles, an area of 5×5 pixels around each particle was selected for secondary processing: by fitting the greyscale values in this area based on a Gaussian distribution, the peak position of the Gaussian distribution was recorded as the particle centre. Theoretically, this method could reach a sub-pixel precision in determining a nanoparticle centre position.

3 SID results

3.1 Measuring the SID

After capturing the greyscale values of all the nanoparticles in the images, the experimental SID $p_{exp}(I)$ was obtained. Figure 3a shows the measured SID histogram of 100-nm particles in 1-mM NaCl solution. In order to fulfil the statistical requirement, approximately 10^5 nanoparticles were counted. Based on our experience in this work, the total number of nanoparticles involved in the statistical analysis should be more than 5×10^4 in order to obtain a reproducible and smooth SID histogram. The x axis of Fig. 3a is the particle intensity I observed from images, which shows the highest observed particle intensity near 1800 and the lowest intensity of approximately 100 close to the image background (after subtracting the background as mentioned in Sect. 2.4). The y axis of Fig. 3a is the value of the measured probability density function $p_{exp}(I)$. Figure 3a shows that the measured $p_{exp}(I)$ manifests a much higher value in the low-intensity range (about $I \sim 100$). The value of $p_{exp}(I)$ decreases rapidly as I increases, and $p_{exp}(I)$ finally presents a low and flat distribution when $I > 1000$. This tendency indicates the intensity decay law of the evanescent field.

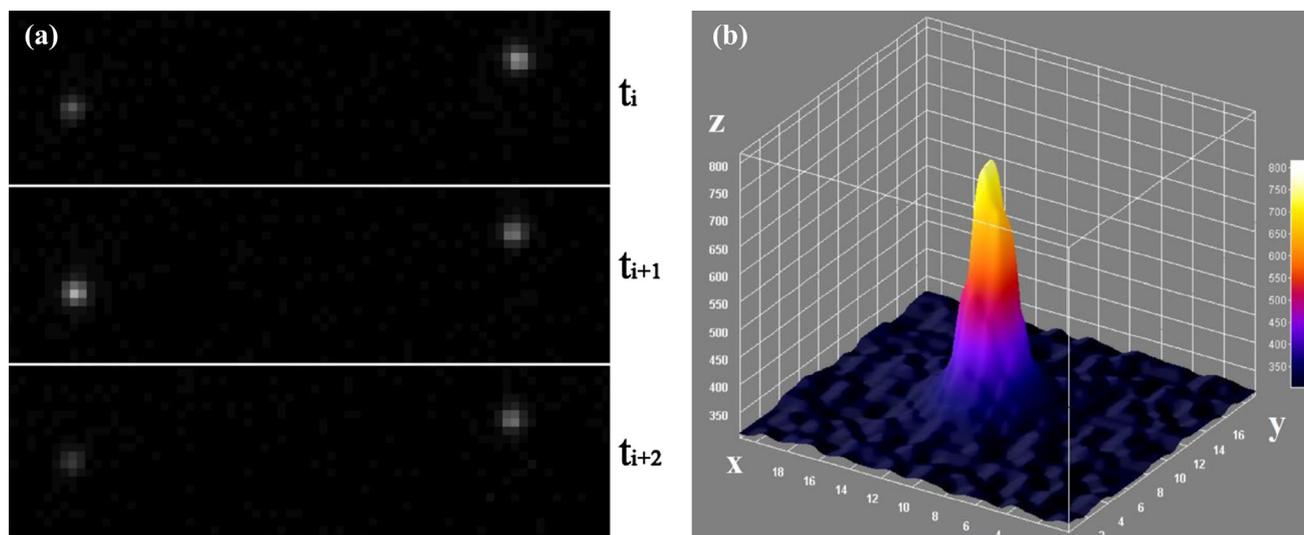**Fig. 2 a** Three successive TIRFM images of 100-nm Brownian nanoparticles emerging during the moment t_i to t_{i+2} (~ 14 ms). **b** The intensity distribution of a nanoparticle exhibits a sharp peak, by which the centre of the nanoparticle can be determined. The z axis is the greyscale value. The nanoparticle spots can be clearly distinguished from the background due to the excellent signal-to-noise ratio
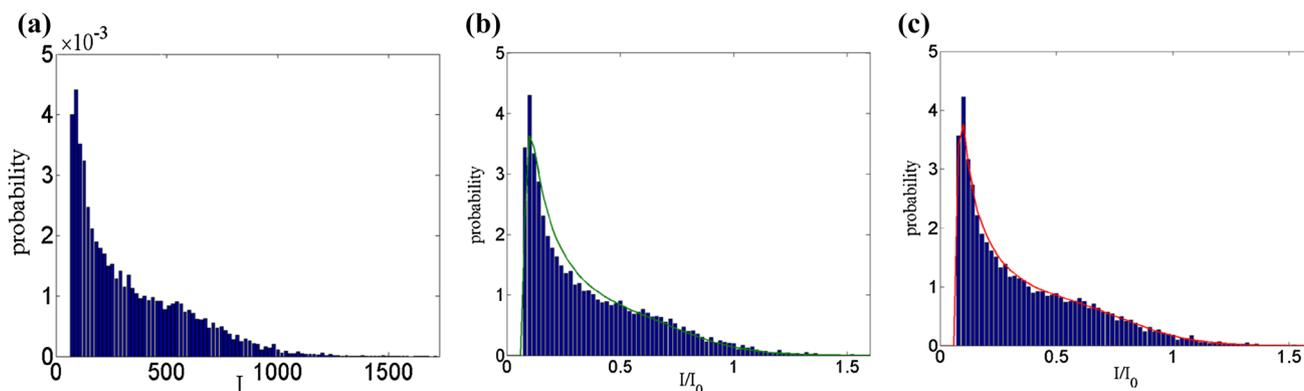
Fig. 3 The measured histogram and the theoretical prediction of the SID using 100-nm nanoparticles in 1-mM NaCl solution ($\kappa^{-1} = 10.0$ nm). **a** The measured intensity probability distribution $p_{\exp}(I)$. **b** The theoretical result of $p_{\mathrm{th}}(I/I_0)$ based on Eq. (5) (the green curve) and the normalized measured data $p_{\exp}(I/I_0)$ from **a**. **c** The the-oretical result of $p_{\mathrm{th}}(I/I_0)$ based on Eq. (8) (the red curve) considering the objective focal plane thickness d_{f}. With the correction based on the focal plane thickness, $p_{\mathrm{th}}(I/I_0)$ is in excellent agreement with the normalized measured data $p_{\exp}(I/I_0)$

3.2 Theoretical model

The measured SID contains rich physics pertaining to the nanoparticle–interface interaction and the properties of nanoparticles. We hereby establish a theoretical model to understand the behaviour of the SID. We first quantitatively describe the particle concentration distribution near the wall. Theoretically, the particle concentration is considered to obey a Boltzmann distribution (Prieve 1999; Banerjee and Kihm 2005; Yoda and Kazoe 2011):

$$C^+(z) = \exp\left(-\frac{\phi(z)}{k_B T}\right), \tag{2}$$

where $C^+(z) = C(z)/C_0$ is the dimensionless particle concentration distribution normalized by the uniform particle concentration C_0 far from the wall, $\phi(z)$ is the potential energy of a nanoparticle at the elevation position z, and $k_B T$ is the thermal energy. Based on the DLVO theory, a full theoretical description of the total potential energy $\phi(z)$ acting on a nanoparticle located at z should contain the electrical double layer repulsion $\phi_E(z)$ and the van der Waals potential $\phi_{vdw}(z)$ (Israelachvili 2011; Banerjee and Kihm 2005; Bouzigues et al. 2008; Zheng and Silber-Li 2009):

$$\phi(z) = \phi_{vdw}(z) + \phi_E(z) = -\frac{A}{6}\left[\frac{a}{z-a} + \frac{a}{z+a} + \ln\left(\frac{z-a}{z+a}\right)\right]$$
$$+ 16\varepsilon a \left(\frac{k_B T}{e}\right)^2 \tan h\left(\frac{e\psi_p}{4k_B T}\right) \tan h\left(\frac{e\psi_w}{4k_B T}\right) e^{-\kappa(z-a)}, \tag{3}$$

where ε is the dielectric permittivity of water, A is the Hamaker constant, a is the mean radius of nanoparticles, ψ_p and ψ_w are the potentials on the respective nanoparticle surface

and wall surface, e is the unit charge, and κ^{-1} is the Debye length characterizing the charge screening effect. It is noteworthy that the expression of $\phi_E(z)$ was deduced based on Derjaguin's approximation, which requires a smaller separation distance $z - a$ than the nanoparticle radius a. For cases where the separation distance $z - a$ is much larger than the nanoparticle radius a, Oberholzer's theory (1997) was proposed to be a better replacement (Wang et al. 2011). However, in the present work, Eq. (3) is found to function more successfully because the nanoparticle radius is not negligible. Therefore, by substituting Eq. (3) into Eq. (2), the equilibrium nanoparticle concentration distribution $C^+(z)$ close to the wall surface is obtained, which also describes the probability that a nanoparticle locates at elevation z from the wall.

Generally, the emission intensity of a fluorescent particle I is assumed to be proportional to the amount of fluorophores within the particle volume, i.e., $I \propto r^3$. Therefore, the particle size influence should be introduced to the intensity exponential decay law (Eq. (1)) to obtain the intensity function $I(r, z)$ of a single nanoparticle:

$$I(r, z) = \left(\frac{r}{a}\right)^3 I_0 \exp\left(-(z-a)/d_p\right). \tag{4}$$

This equation demonstrates the intensity of a particle with radius r and location at elevation z. Its normalized form is:

$$\frac{I(r, z)}{I_0} = \left(\frac{r}{z}\right)^3 \exp(-(z-a)/d_p). \tag{5}$$

We further consider the poly-dispersity of nanoparticles. The probability distribution of particle radius r takes the form of a Gaussian distribution:

$$p(r) = \frac{1}{\sqrt{2\pi}\sigma} \exp\left(-\frac{(r/a-1)^2}{2\sigma^2/a^2}\right), \qquad (6)$$

where a represents the mean particle radius and σ is the standard deviation. Substituting Eq. (5) into Eq. (6), a joint probability density function for particle intensity I and elevation z is provided as:

$$p(I,z) = \frac{1}{\sqrt{2\pi}\sigma} \exp\left(-\frac{\left[\left(\frac{I}{I_0 E_{\text{decay}}(z)}\right)^{\frac{1}{3}} - 1\right]}{2\sigma^2/a^2}\right), \qquad (7)$$

where $E_{\text{decay}}(z) = \exp(-(z-a)/d_p)$, is a decay function characterizing the exponential evanescent wave field. Therefore, by combining Eqs. (2), (3) and (7), we are able to obtain the theoretical probability distribution $p_{th}(I)$ to describe the implied physics of the SID. One advantage of this method is that I_0 is the only unknown parameter in these equations to be determined by fit.

3.3 Determining I_0

The deduction above shows that the theoretical intensity distribution can be solved based on a Boltzmann distribution (Eqs. (2) and (3)) and the joint probability distribution Eq. (7). However, obtaining an analytical solution is very difficult. We here employ a numerical method to solve the intensity distribution probability SID (see section S3 of the Online Resource ESM_1.pdf for details). The green curve in Fig. 3b shows the theoretical curve of $p_{th}(I/I_0)$ as a function of I/I_0 for 100-nm particles in 1-mM NaCl solutions. In the numerical solving process, the Debye length is $\kappa^{-1} = 10$ nm, the mean diameter of the nanoparticles is $2a = 103.5$ nm, the particle size variation $\sigma = 6.3\%$, and the particle surface potential $\psi_p = -46.5$ mV (as provided in Table 1). The glass wall surface potential $\psi_w = -27.0$ mV was measured from electroosmosis measurement.

The measured histogram of the SID and the theoretical curve of the SID (the green curve in Fig. 3b) have the same shape, so it is possible to determine I_0 based on least square regression. The procedure is as follows: (a) an initial value of I_0 is given for trial calculation. Then, the probability of each column $[p_{\text{exp}}(I_j)$ corresponding to $I_j]$ in Fig. 3a is normalized to $p_{\text{exp}}(I_j/I_0)$. Based on the requirement of the probability density function, $\sum_j p_{\text{exp}}(I_j/I_0) = 1$ should always be fulfilled. (b) The relative deviation r_j between the measured probability $p_{\text{exp}}(I_j/I_0)$ and the theoretical estimated probability $p_{th}(I_j/I_0)$ is calculated as: $r_j = p_{\text{exp}}(I_j/I_0) - p_{th}(I_j/I_0)$. The residual error S is defined as: $S = \sum_j r_j^2$. (c) The program

will search for the "best" I_0 by changing the initial value with a step of five units of the grey-scale value. The "best" I_0 means the least corresponding residual error S. For the measured data shown in Fig. 3b (100-nm nanoparticles in 1-mM NaCl solution), we can obtain $I_0 = 920$ by least square regression.

Furthermore, we want to emphasize that $I_0 = 920$ determined by the SID method is obviously smaller than the brightest particle intensity observed in the experiment, which is $I_{\text{max}} = 1752$. This deviation indicates that simply using the intensity of the brightest particle near or attached to the wall as I_0 will introduce a large error in determining I_0 and the particle's z position. The result that I_{max} is much larger than I_0 in fact arises from the particle size variation, as described by the term $(r/a)^3$ in Eq. (5).

3.4 The influence of the objective focal plane thickness

The measured probability $p_{\text{exp}}(I/I_0)$ in the range of $0.15 < I/I_0 < 0.5$ in Fig. 3b is still lower than the theoretical curve $p_{th}(I/I_0)$. This implies that additional influences decreasing the observed intensity should be taken into account. It has been known that in microscopic observation, the particle intensity will decrease if it moves away from the focal plane (Li et al. 2014; Joseph and Tabeling 2005; Zheng et al. 2013). Therefore, in TIRFM measurement, the nanoparticle intensity is influenced not only by the evanescent field but also by the position of the objective focal plane. The Lorentzian distribution is usually used to describe the intensity variation near the focal plane (Joseph and Tabeling 2005; Loppinet et al. 2012; Zheng et al. 2013), and thus, Eq. (5) becomes:

$$\frac{I(r,z)}{I_0} = \left(\frac{r}{a}\right)^3 \exp(-(z-a)/d_p)\frac{1}{1+\left(\frac{z-z_f-a}{d_f}\right)}, \qquad (8)$$

where z_f is the position of the objective focal plane ($z_f = 0$ because the focal plane was adjusted to the wall surface in the experiment) and d_f is the thickness of the focal plane, which can be estimated by the equation of depth of field $d_f = \frac{n\lambda}{\text{NA}^2} + \frac{nk}{M \cdot \text{NA}}$ (Meinhart et al. 1999). In this equation, $n = 1.518$ is the refractive index of the objective, $\lambda = 488$ nm is the wave length of the incident laser, $\text{NA} = 1.45$ is the numerical aperture of the objective, $M = 100$ is the magnification of the objective, and $k = 8$ μm is the pixel size of the EMCCD sensor. According to these parameters, we obtain the theoretical $d_f = 350$ nm. In the experiment, we also measured the focal plane thickness d_f. The method was to fit the intensity variation of a nanoparticle attached to the wall by changing the position of the focal plane via a piezotransducer (section S4 of the Online Resource ESM_1.pdf).

The measurement showed that the focal plane thickness was $d_f = 420$ nm. Note that the influence of the focal plane cannot be neglected because the typical length scales d_p and d_f are close. In Fig. 3c, the fit result based on Eq. (8) taking the objective focal plane into account is shown. It is clear that Fig. 3c shows a much better fit when compared to Fig. 3b (the least residual error S is reduced by about 80%), and we obtain $I_0 = 945$. Only by considering the Lorentzian distribution in Eq. (8), the profile of the measured probability can be demonstrated appropriately. In all the measurements of this study, considering the focal plane effect always results in a better fit and a more accurate result.

4 The applications of the SID method

We have established a full description of the SID and have proposed a novel method to determine I_0 based on the statistical intensities of a large amount of nanoparticles emerging in the evanescent field. In this section, the validity and precision of this method will first be examined by velocity measurements near the wall. We will show that the precision of determining z positions of nanoparticles is significantly improved. Second, the results of the SID are shown to be sensitive to properties of the electric double layer and the nanoparticle.

4.1 Near-wall velocity measurement by nanoPTV

We applied the SID method of determining I_0 to the near-wall velocity measurement (Online Resource ESM_4.avi). The experimental setup was similar to the one introduced in Sects. 2.1–2.3. The only difference was that a microfluidic flow control system (Fluigent MFCS) was used to generate stable pressure ($\Delta p = 2.0$ kPa) to drive the flow in the PDMS microchannel. The observation region was still located at the channel centre close to the glass surface. The size of the region was 24.0 µm along the channel streamwise direction (defined as x) and 12.8 µm along the channel spanwise direction (defined as y). In the experiment, the exposure time and the interval time between two successive frames remained at $t_e = 0.4$ ms and $\Delta t = 7$ ms. In the same position, the frame number of an image series increased to 10,000 instead of 1000. Five image series were taken in five different positions under the same experimental conditions. Because the nanoparticle would move with the fluid flow, the total time during which it remained in the laser-illuminated region lasted only about 10 ms. Thus, the influence of photobleaching was neglected in the velocity measurement.

After the measurement and image processing, the base intensity I_0 of each case was determined based on the SID method described in Sects. 3.2–3.4. The vertical z position of each nanoparticle was then calculated according to Eq. (8). The velocity data were obtained based on the nanoPTV method. The coordinates of a single nanoparticle appearing in the image at the moment t were known as (x_t, y_t, z_t). After a time interval Δt, these coordinates became ($x_{t+\Delta t}$, $y_{t+\Delta t}$, $z_{t+\Delta t}$). Therefore, the measured velocity of this nanoparticle during Δt was calculated as $V_{exp} = (x_{t+\Delta t} - x_t)/\Delta t$, and the vertical location z_V of this velocity vector was defined at the centre of the displacement: $z_V = (z_t + z_{t+\Delta t})/2$. After measuring V_{exp} and z_V of all the observed nanoparticles, we obtained the measured velocity profile based on the scattered velocity data (Fig. 4a shows an example using 250-nm particles in 1-mM NaCl solutions). The scattered red circles are distributed in a band with a half width of $\Delta V = \pm 50$ µm/s around the blue line. This scattered distribution randomly located close to the theoretical line is due to the influence of particle Brownian
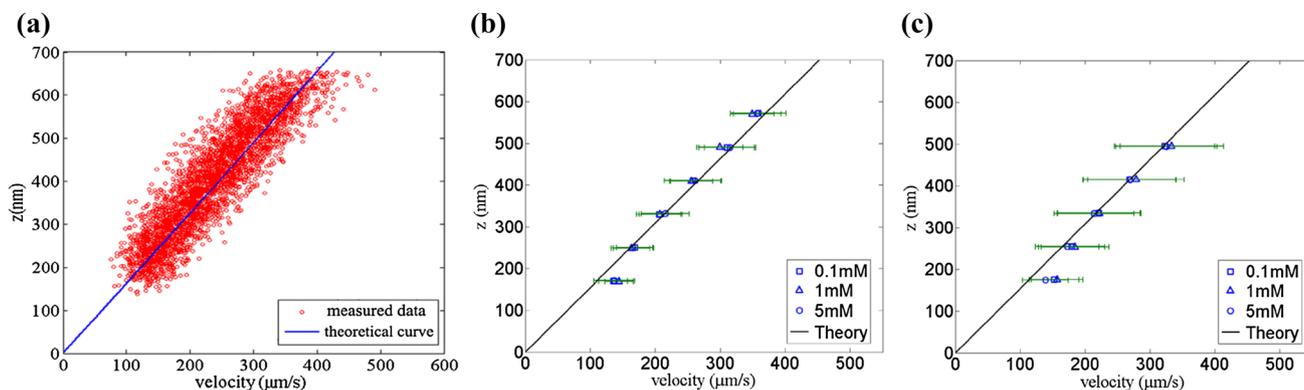

Fig. 4 Measured velocity profiles using nanoPTV. **a** The scattered velocity data using 250-nm particles in 1-mM NaCl solution. **b** and **c** The measured multi-layer velocity profiles using 250-nm or 100-nm particles, respectively. The blue symbols (rectangles for 0.1 mM, triangles for 1 mM, and circles for 5 mM) are the mean values of the measured data in different layers. The solid lines in the three plots are the theoretical curves based on Eq. (9)

motion. According to $u_{Br} = 2\sqrt{D/\Delta t}$ (where D is the diffusion coefficient of the tracers), calculating the mean velocity of particle Brownian motion, we estimate the contribution of Brownian motion on the measured velocity to be approximately ± 42 μm/s, which is consistent with the half band width of the measured data. Therefore, the fluctuation of the measured velocity is mainly influenced by the random Brownian motion of the nanoparticles.

The measured velocity is compared with the theoretical solution of the Navier–Stokes equation with the no-slip boundary condition applied. The theoretical velocity distribution $V_{th}(y,z)$ in a channel with rectangular cross section is (White 1974; Zheng et al. 2013):

$$V_{th}(y,z) = \frac{4h^2 \Delta p}{\pi^3 \mu L} \sum_{n=1,3,5...}^{\infty} \frac{1}{n^3} \left[1 - \frac{\cos h\left(n\pi \frac{y}{h}\right)}{\cos h\left(n\pi \frac{w}{2h}\right)} \right] \sin \left(n\pi \frac{z}{h}\right),$$

(9)

where μ is the viscosity; L, h and w are the length, the height and the half width of the channel; and n is an integral of the series. We then calculated the average velocities from the scattered data in every layer with a thickness of 80 nm. Figure 4b, c manifests the multi-layer velocity profiles using 250-nm and 100-nm particles, respectively. The error bars are calculated based on the standard deviations of measured velocities, which are approximately 13–21% of the average values. The standard deviations from the scattered data indicate the influence of Brownian motion. By calculating the statistical mean, the influence of Brownian motion can be eliminated from the velocity measured data. Figure 4 shows that the measured velocities are in excellent agreement with the theoretical prediction. This result indicates that the SID method displays good precision in determining I_0 and the vertical z particle positions. Thus, our SID method provides a helpful tool to solve the problem of high uncertainty in nanoPTV measurements (see section S5 of the Online Resource ESM_1.pdf for more details).

4.2 The influence of the salt concentration

We will further show the dependence of the SID on the salt concentration. We measured the SID of nanoparticles in the NaCl solutions with different concentrations (0.1 mM, 1 mM and 5 mM). Based on the method described above, I_0 was determined. The influence of the focal plane was also considered, and thus, the theoretical curve was solved based on Eq. (8). Figure 5a, b, respectively, shows the measured histograms of $p_{exp}(I/I_0)$ and the corresponding fitting theoretical curves $p_{th}(I/I_0)$ in 0.1-mM and 5-mM NaCl solutions using 100-nm particles. The parameters adopted in the theoretical model are shown in Table 1. Comparing the results in Fig. 3 (1 mM) and Fig. 5 (0.1 mM and 5 mM), we can see that the peak of the probability distribution is always located around $I/I_0 = 0.1$ and that the probability value decreases with increasing intensity. This common tendency is determined by the typical intensity decay law of the evanescent field. As I/I_0 increases, an extrusion appears at $0.5 < I/I_0 < 0.7$ in the cases using higher concentration solutions (i.e., 1 mM in Figs. 3c, 5 mM in Fig. 5b). The higher the concentration used, the more clearly the extrusion can be observed. The Debye length κ^{-1} is the typical length scale of the electrostatic repulsion, which is closely related to the salt concentration. The Debye lengths of 0.1-mM, 1-mM and 5-mM NaCl solutions are measured to be approximately 31.4 nm, 10.0 nm and 4.6 nm. This indicates that the particle concentration decreases significantly due to the electrostatic repulsion only within approximately 10–100 nm of the wall. Therefore, in 5-mM solution (Fig. 5b, $\kappa^{-1} = 4.6$ nm), the SID shows a step-like sudden decrease close to $I/I_0 = 1$, indicating the decrease in the particle concentration occurring within $z \sim 10$ nm from the wall. In contrast, in the case of low salt concentration (0.1 mM in Fig. 5a, $\kappa^{-1} = 31.4$ nm), the decrease in SID due to electrostatic repulsion appears over a wider range ($0.7 < I/I_0 < 1$) and shows a gentler slope.

The results above reveal that the SIDs are sensitive to the salt concentration (or Debye length κ^{-1}). Recalling the Boltzmann distribution (Eqs. (2) and (3)), we can see that

Fig. 5 The measured histograms of SID $p_{exp}(I/I_0)$ and the corresponding fitting theoretical curves $p_{th}(I/I_0)$ (red curve) in **a** 0.1-mM and **b** 5-mM NaCl solutions using 100-nm particles
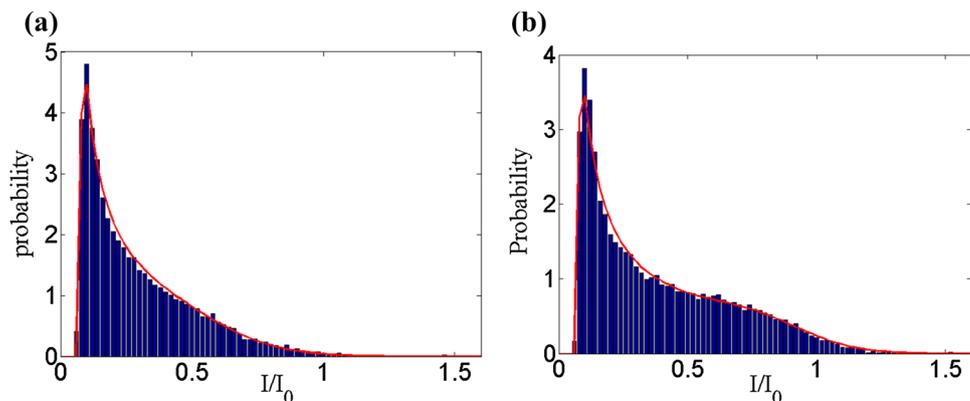
the concentration distribution is mainly influenced by the electrical double-layer repulsion ϕ_E. In the component of ϕ_E in Eq. (3), the major terms are the one containing the Debye length κ^{-1} and the one describing the particle size a, while the hyperbolic tangent terms related to the particle and wall surface potential only contribute to a small extent. Because the Debye length κ^{-1} is in the exponential term, its variation from a few nanometres to 100 nm results in a variation of φ_E of three orders of magnitude. Thus, the Debye length, which directly corresponds to the salt concentration, is the most important factor. This result explains why a small change in salt concentration (or the Debye length) could result in a clear variation of the SID. It also evokes the potential of a novel nano-probe based on the SID to detect the solution concentration of colloidal properties in nanoscale confinements (Bevan and Eichmann 2011). For instance, after I_0 has been determined, other parameters such as the Debye length κ^{-1} can be detected by fitting the measured SID histogram with the theoretical model above.

5 Conclusions

In summary, we investigated the statistical intensity distribution (SID) of fluorescent nanoparticles in the evanescent field by TIRFM. We established the theoretical description of the SID by considering the Boltzmann distribution of nanoparticle concentration, the statistical particle size variation, and the influence of the objective focal plane thickness. We report excellent consistency between the measured SID histogram and the theoretical description. We then developed a method to precisely determine the base intensity I_0 and decode nanoparticle vertical z positions, by which the measurement uncertainty of TIRFM can be significantly reduced. The merit of our SID method is that I_0 is the only fit parameter, compared to the previous method (Li et al. 2014) with more than four fit parameters. We have proved the accuracy of our method by nanoPTV near-wall velocity measurement. The results indicate that simply using the intensity of the brightest particle near or attached to the wall as I_0 will introduce a large error in determining I_0 and the particle's z position. Our SID method is shown to be valid using nanoparticles whose diameters are larger than approximately 100 nm. The lower limit of the nanoparticle diameter is still under investigation, as the limit of Derjaguin's approximation and the strong Brownian motion will introduce larger uncertainty when smaller nanoparticles are used. We further unveil the physical insight of the SID, which is found to be sensitive to the salt concentration (or the Debye length) of the solution. This result implies the possibility of measuring SID as a nano-probe to investigate solution or colloidal properties in nanofluidics. Furthermore, by establishing the SID near the interface, the current method has the potential to be applied to detect the fluorescence signals of the biomolecules covering the interface.

References

Banerjee A, Kihm KD (2005) Experimental verification of near-wall hindered diffusion for the Brownian motion of nanoparticles using evanescent wave microscopy. Phys Rev E 72:42101

Bevan M, Eichmann S (2011) Optical microscopy measurements of kT-scale colloidal interactions. Curr Opin Colloid Interface Sci 16:149–157

Bliokh KY, Bekshaev AY, Nori F (2014) Extraordinary momentum and spin in evanescent waves. Nat Commun 5:3300

Bouzigues CI, Tabeling P, Bocquet L (2008) Nanofluidics in the Debye layer at hydrophilic and hydrophobic surfaces. Phys Rev Lett 101(11):114503

Chan C, Ohl C (2012) Total-internal-reflection-fluorescence microscopy for the study of nanobubble dynamics. Phys Rev Lett 109:174501

Choi CK, Margraves CH, Kihm KD (2007) Examination of near-wall hindered Brownian diffusion of nanoparticles: Experimental comparison to theories by Brenner (1961) and Goldman et al. (1967). Phys Fluids 19(10):103305

Fan YJ, Sheen HJ, Chen ZY, Liu YH, Tsai JF, Wu KC (2015) TIRF-enhanced nanobeads' Brownian diffusion measurements for detecting CRP in human serum. Microfluid Nanofluid 19(1):85–94

Hertlein C, Riefler N, Eremina E, Wriedt T, Eremin Y, Helden L, Bechinger C (2008) Experimental verification of an exact evanescent light scattering model for TIRM. Langmuir 24(1):1–4

Huang P, Guasto JS, Breuer KS (2006) Direct measurement of slip velocities using three-dimensional total internal reflection velocimetry. J Fluid Mech 566:447–464

Israelachvili J (2011) Intermolecular and surface forces. 3rd edn. Academic Press, New York

Joseph P, Tabeling P (2005) Direct measurement of the apparent slip length. Phys Rev E 71:035303

Kazoe Y, Yoda M (2011) Measurements of the near-wall hindered diffusion of colloidal particles in the presence of an electric field. Appl Phys Lett 99(12):124104

Kihm KD, Banerjee A, Choi CK, Takagi T (2004) Near-wall hindered Brownian diffusion of nanoparticles examined by three-dimensional ratiometric total internal reflection fluorescence microscopy (3-D R-TIRFM). Exp Fluids 37(6):811–824

Li Z, D'eramo L, Lee C, Monti F, Yonger M, Tabeling P, Chellet B, Bresson B, Tran Y (2014) Near-wall nanovelocimetry based on total internal reflection fluorescence with continuous tracking. J Fluid Mech 766:147–171

Loppinet B, Dhont JKG, Lang P (2012) Near-field laser Doppler velocimetry measures near-wall velocities. Eur Phys J E 35:62

Madariaga-Marcos J, Hormeno S, Pastrana CL, Fisher GLM, Dillingham MS, Moreno-Herrero F (2018) Force determination in lateral magnetic tweezers combined with TIRF microscopy. Nanoscale 10(9):4579–4590

McKee CT, Clark SC, Walz JY, Ducker WA (2005) Relationship between scattered intensity and separation for particles in an evanescent field. Langmuir 21(13):5783–5789

Meinhart CD, Wereley ST, Santiago JG (1999) PIV measurement of a microchannel flow. Exp Fluids 25:414–419

Oberholzer MR, Wagner NJ, Lenhoff AM (1997) Grand canonical Brownian dynamics simulation of colloidal adsorption. J Chem Phys 107:9157–9167

Prieve DC (1999) Measurement of colloidal forces with TIRM. Adv Colloid Interface Sci 82:93–125

Prieve DC, Frej NA (1990) Total internal reflection microscopy: a quantitative tool for the measurement of colloidal forces. Langmuir 6(2):396–403

Qian B, Park J, Breuer KS (2015) Large apparent slip at a moving contact line. Phys Fluids 27(9):091703

Shin DH, Marnun M, Almonte J, Margraves CH, Kang YT, Lee SH, Choi CK (2016) A noninvasive method to predict fluid viscosity and nanoparticle size using total internal reflection fluorescence microscopy (TIRFM) imaging. Microfluid Nanofluid 20(3):45

Squires TM (2017) Micro-plumes for nano-velocimetry. J Fluid Mech 832:1–4

Wang W, Huang P (2016) Hybrid algorithm for extracting accurate tracer position distribution in evanescent wave nano-velocimetry. Exp Fluids 57(2):27

Wang W, Guasto JS, Huang P (2011) Measurement bias in evanescent wave nano-velocimetry due to tracer size variations. Exp Fluids 51(6):1685–1694

Wereley ST, Meinhart CD (2010) Recent advances in micro-particle image velocimetry. Annu Rev Fluid Mech 42:557–576

White FM (1974) Viscous fluid flow. McGraw-Hill Book Company, New York, p 123

Wu HJ, Bevan MA (2005) Direct measurement of single and ensemble average particle-surface potential energy profiles. Langmuir 21(6):1244–1254

Yoda M, Kazoe Y (2011) Dynamics of suspended colloidal particles near a wall: Implications for interfacial particle velocimetry. Phys Fluids 23(11):111301

Zetterner C, Yoda M (2003) Particle velocity field measurements in a near-wall flow using evanescent wave illumination. Exp Fluids 34(1):115–121

Zheng X, Silber-Li Z (2008) Measurement of velocity profiles in a rectangular microchannel with aspect ratio α = 0.35. Exp Fluids 44:951–959

Zheng X, Silber-Li Z (2009) The influence of Saffman lift force on nanoparticle concentration distribution near a wall. Appl Phys Lett 95(12):124105

Zheng X, Kong G, Silber-Li Z (2013) The influence of nano-particle tracers on the slip length measurements by microPTV. Acta Mech Sin 29(3):411–419

Zheng C, Zhao GY, Liu WJ, Chen YH, Zhang ZM, Jin LH, Xu YK, Kuang CF, Liu X (2018) Three-dimensional super resolved live cell imaging through polarized multi-angle TIRF. Opt Lett 43(7):1423–1426